Long-term calcium imaging reveals functional development in hiPSC-derived cultures comparable to human but not rat primary cultures

Estefanía Estévez-Priego,[1,2,6,*] Martina Moreno-Fina,[1] Emanuela Monni,[3] Zaal Kokaia,[3] Jordi Soriano,[1,2,7] and Daniel Tornero[4,5,7,*]

[1]Departament de Física de la Matèria Condensada, Universitat de Barcelona, 08028 Barcelona, Spain
[2]Universitat de Barcelona Institute of Complex Systems (UBICS), 08028 Barcelona, Spain
[3]Laboratory of Stem Cells and Restorative Neurology, Lund Stem Cell Center, Department of Clinical Sciences, Lund University, 22184 Lund, Sweden
[4]Laboratory of Neural Stem Cells and Brain Damage, Department of Biomedical Sciences, Institute of Neurosciences, University of Barcelona, 08036 Barcelona, Spain
[5]August Pi i Sunyer Biomedical Research Institute (IDIBAPS), 08036 Barcelona, Spain
[6]Present address: Universidad Politécnica de Madrid – Life Supporting Technologies Research Group, ETSIT, 28,040, Madrid, Spain
[7]Co-senior authors
*Correspondence: eestevez@lst.tfo.upm.es (E.E.-P.), daniel.tornero@ub.edu (D.T.)
https://doi.org/10.1016/j.stemcr.2022.11.014

SUMMARY

Models for human brain-oriented research are often established on primary cultures from rodents, which fails to recapitulate cellular specificity and molecular cues of the human brain. Here we investigated whether neuronal cultures derived from human induced pluripotent stem cells (hiPSCs) feature key advantages compared with rodent primary cultures. Using calcium fluorescence imaging, we tracked spontaneous neuronal activity in hiPSC-derived, human, and rat primary cultures and compared their dynamic and functional behavior as they matured. We observed that hiPSC-derived cultures progressively changed upon development, exhibiting gradually richer activity patterns and functional traits. By contrast, rat primary cultures were locked in the same dynamic state since activity onset. Human primary cultures exhibited features in between hiPSC-derived and rat primary cultures, although traits from the former predominated. Our study demonstrates that hiPSC-derived cultures are excellent models to investigate development in neuronal assemblies, a hallmark for applications that monitor alterations caused by damage or neurodegeneration.

INTRODUCTION

The limited availability of human brain tissue for research studies has required the use of many different models to mimic physiological and pathological conditions of the CNS development. Animal models have been useful to investigate brain disease mechanisms and potential treatments but frequently failed during translation onto human diseases, probably due to the considerable differences in complexity between the human and rodent brains, with the latter being one of the most used models in neuroscience research.

The advent of human induced pluripotent stem cells (hiPSCs) (Takahashi et al., 2007) has revolutionized the possibilities of *in vitro* models to study the human brain, presenting enormous potential for disease modeling and drug screening (Petros et al., 2011). During the last 10 years, many studies using hiPSC-derived neural cultures have established *in vitro* systems that more reliably identify molecular pathways and predict effective drug targets for neurological disorders (Park et al., 2008; Bellin et al., 2012; Shi et al., 2012; Inoue et al., 2014). Exhaustive morphological, biochemical, and functional characterization of neuronal cultures is needed to detect phenotypical differences between healthy and diseased cells. Up to this point, some limitations of these *in vitro* models have been

tied to the lack of tools to study neuronal circuits at a mesoscopic scale and extract reliable neuronal functional features.

Indeed, important network aspects such as self-organization (Pasquale et al., 2008), activity patterns (Chiappalone et al., 2006), synchronization (Eytan and Marom, 2006; Schroeter et al., 2015), mesoscale architecture (Okujeni and Egert, 2019; Tibau et al., 2020), the emergence of spontaneous activity (Orlandi et al., 2013), or functional network formation (Poli et al., 2015; Schroeter et al., 2015) have been widely studied in rodent primary cultures, both in two-dimensional (2D) and three-dimensional (3D) preparations (Dingle et al., 2020), providing invaluable insight on the functional organization of neuronal circuits. However, it is not clear whether such investigations apply to hiPSCs network formation and functionality. Recent studies have studied in detail the development of activity and functional connectivity in hiPSCs (Kirwan et al., 2015), but a detailed comparison of the behavior of hiPSCs and rat primary cultures has been started only recently, depicting important differences both in 2D (Hyvärinen et al., 2019) and 3D (Koroleva et al., 2021).

Here, we apply advanced computational tools to demonstrate that hiPSC-derived neural cultures can reach important levels of neuronal activity and functional richness, with processes that are similar to those occurring during
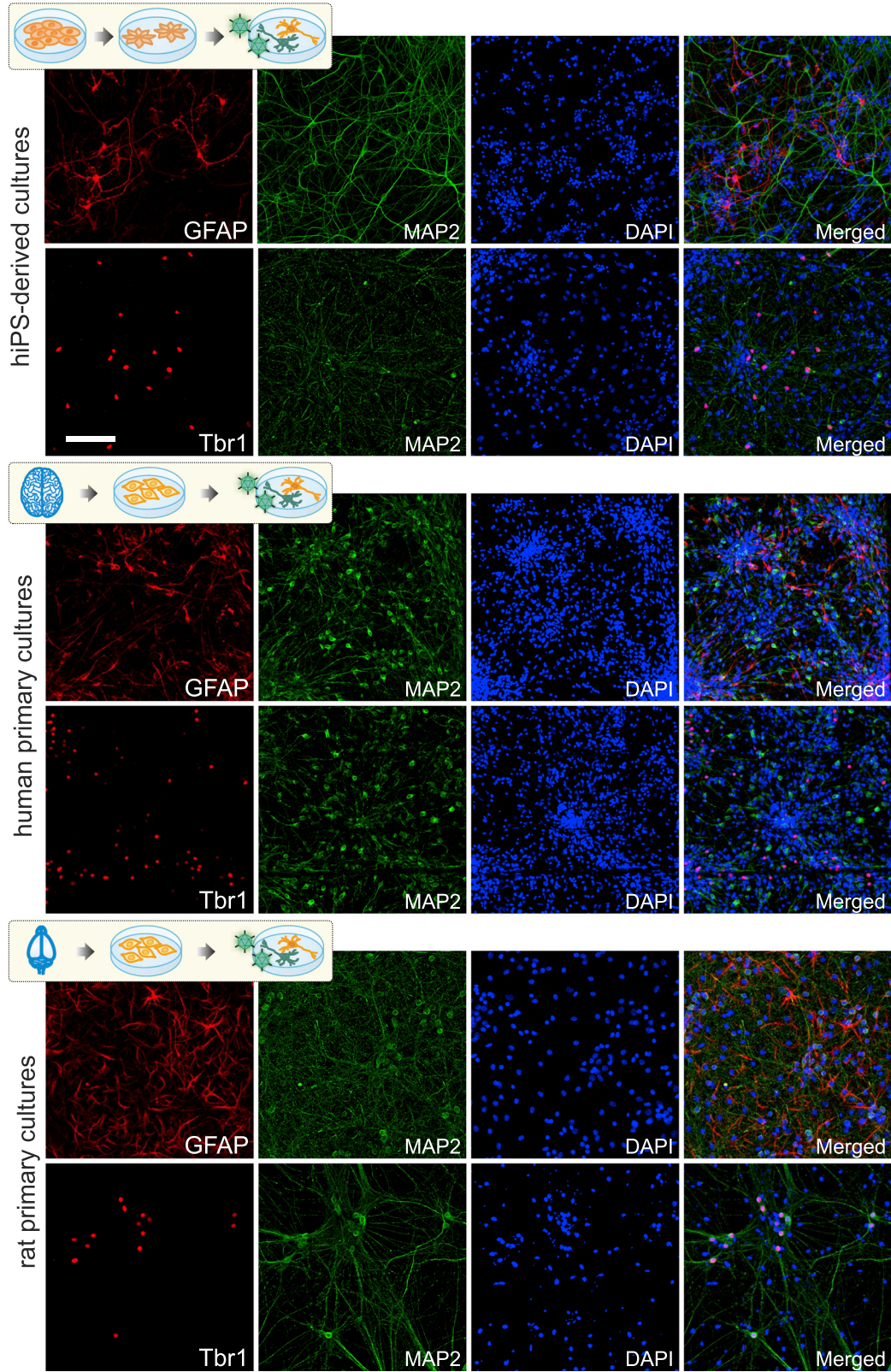
(legend on next page)

brain development and network establishment. Our results show that these cultures behave differently from rat brain neuronal primary cultures and are very similar to primary cultures derived from human embryonic cortical progenitors. We described several characteristics of the networks that are specific to human neurons and can be used to evaluate possible defects in neuronal function derived from neurological diseases.

RESULTS

Generation of comparable neural cultures

Mature neural cultures were generated from hiPSCs-derived progenitors, while human and rat primary cultures were obtained from the cortex of human and rat embryos in similar conditions. All three types of cultures were tracked during a fixed range of days, counted based on the differentiation day (DD). In the case of hiPSC-derived cultures, DD0 corresponds to the withdrawal of the growth factors that maintain the progenitors in the proliferative state. In the case of the primary cultures, human or rat, DD0 corresponds to the day of plating. Human cultures, hiPSC-derived and primary, exhibited an optimal density and a homogeneous distribution within a temporal range from DD15 to DD55, while in rat primary cultures, neural network development was observed from DD4 to DD17, presenting a much shorter lifespan.

Biochemical characterization at the final time point for all kinds of cultures under study (DD50–55 for hiPSC-derived and human primary, and DD17 for rat primary cultures) revealed the presence of approximately 70% of cells positive for mature neuronal marker MAP2 (microtubule-associated protein 2) and around 10% of reactive astrocytes immunopositive for GFAP (glial fibrillary acidic protein) (Figure 1, top panels for each type of culture). Among mature neurons (MAP2-positive), the majority of the cells were also immunoreactive against cortical specific markers such as TBR1 (Figure 1, lower panels for each type of culture). Human-derived astrocytes showed longer ramifications than rat-derived ones, resulting in a higher area of the neuronal culture covered by each astrocyte (GFAP staining in Figures 1 and S1A–S1C).

After infection with adeno-associated virus (AAV) carrying the genetically encoded calcium indicator (GECI) GCaMP6s under the control of Synapsin I promoter,

around 50% of the neurons expressed the protein as evidenced by calcium level recordings and immunocytochemistry at the final time point for all types of cultures (see Figure S1D).

Dynamic monitorization of neuronal activity reveals differences between the cultures

GECI expression makes it possible to monitor intracellular calcium levels in cultures during the generation and maturation of neuronal networks. Recordings were carried out every 3–4 days in the different types of cultures, hiPSC-derived, human primary, and rat primary cultures. The use of glass-bottom plates with a grid allowed us to record at the different time points from the same regions of the plate, reducing the variability related to culture heterogeneity. The first obvious difference between the three types of cultures was the timescales of culture development in terms of survival limitations, but also regarding the arousal of neuronal activity. While human cultures (iPSC-derived and primary) exhibited neuronal activity at day 20, rat primary cultures showed it already from day 4. Activity monitoring was stopped at days 55 and 17, respectively, since the dynamic behavior of the cultures did not appreciably change any longer. To overcome this misalignment in timescales, we defined three well-distinguishable stages, allowing the interpolation of timelines and facilitating the comparison of functional development traits. "Early" corresponds to the first 1–3 days following the beginning of GCaMP6s expression (DD20–25 for human cultures and DD5–7 for rat primary cultures). "Intermediate" corresponds to fully active yet young networks approximately at the midpoint of the tracking protocol (DD26–40 for human cultures and DD8–14 for rat primary cultures). And "Late" corresponds to well-matured functional networks by the end of the tracking protocol (DD41–55 for human cultures and DD14–17 for rat primary cultures). Representative fluorescence traces at these three stages for the three types of cultures (Figure 2) evidenced a different pattern of activity mainly between human and rat cultures. In hiPSC-derived cultures, neurons were practically silent during the early stage, although expression of GCaMP6s was sufficient to identify cell bodies (Figure 2A, top panel). Gradually, hiPSC-derived neurons built up spiking activity and, at intermediate stages, showed rich activity characterized by a combination of sporadic (black arrowheads) and

---

Figure 1. Characterization of cell cultures

Representative fluorescent photomicrographs showing the expression of neural markers in hiPSC-derived cultures (top panel), human primary cultures (middle panel), and rat primary cultures (bottom panel), all at the final time point (DD55, DD50, and DD17, respectively). For each of the three conditions, the top picture shows the expression of glial marker GFAP (in red), mature neuronal marker MAP2 (in green), and nuclear marker DAPI (in blue), while the bottom picture shows the expression of cortical marker TBR1 (in red), mature neuronal marker MAP2 (in green), and nuclear marker DAPI (in blue). Scale bar represents 100 μm.
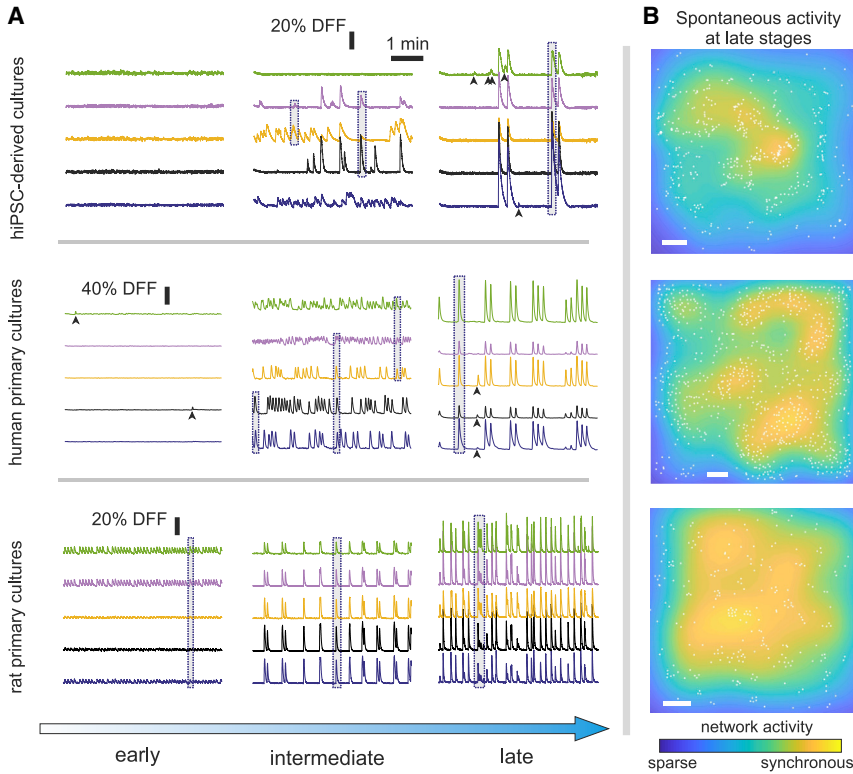
A

hiPSC-derived cultures

20% DFF ▮ ▬ 1 min

human primary cultures

40% DFF ▮

rat primary cultures

20% DFF ▮

early → intermediate → late

B Spontaneous activity at late stages

network activity

sparse → synchronous

Figure 2. Calcium imaging and emergence of collective activity

(A) Representative fluorescence traces of five neurons for early, intermediate, and late developmental stages. The set of traces corresponds to the same monitored neurons. Dashed blue boxes highlight coordinated activity and black arrowheads sporadic events.

(B) The spatial extent of synchronous spontaneous activity at the last stage of development in a representative experiment for each condition. Scale bar represents 200 μm.

correlated activations, i.e., collective synchronous events (blue dashed boxes). Network activity became strongly synchronous at late stages, although some sporadic activations and non-fully synchronous events coexisted (black arrowheads). For human primary cultures, networks were also practically silent in the early stages, but within a week, they evolved toward a highly active network in which correlated events with different participating neurons were present, as illustrated by the dashed boxes at the intermediate stage (Figure 2A, middle panel). At late maturation stage, the network generated by human primary cultures became fully synchronous, while sporadic events were rare. In rat primary cultures, activity was pronounced as soon as GCaMP6s expression allowed to observe calcium transients, with most of the neurons firing together already at early stages (Figure 2A, bottom panel). This strong synchronization was maintained in intermediate and late stages, shaping a very rigid network.

At late stages, all three culture types analyzed showed rich network activity, which covered the entire area of the culture as evidenced by the spatial distribution of activity (Figure 2B), where yellow areas depict regions with the strongest coordinated activity. For hiPSC-derived cultures, the observed hybrid pattern of synchronous and sporadic events translates into smaller areas of coordinated activity, and therefore the yellow spot is relatively small in exten-

sion. However, for human and rat primary cultures, yellow areas cover most of the network, indicating that these cultures were strongly locked in a synchronous dynamic regime.

Collective activity analysis revealed richer dynamics in human-derived cultures

To further investigate the development of activity in the different types of cultures, we generated raster plots and analyzed the strength of population activity during network maturation at the different stages (Figure 3A). Strength of population activity (upper part of each panel, in red) quantifies the fraction of neurons in the network that activated together in a short time window. The height of the peaks indicated the fraction of neurons in the network that participated in a collective event, with strongly synchronous dynamics corresponding to peaks close to 1. For hiPSC-derived cultures (Figure 3A, top panel), activity at early stages was essentially sporadic, and therefore the population activity was low. The presence of coordinated activity at intermediate stages was revealed by synchronous events in the raster plot and that corresponded to sharp peaks in population activity. The number of peaks substantially increased at late stages of development in hiPSC-derived cultures. However, the height of these peaks varied along with the recording,
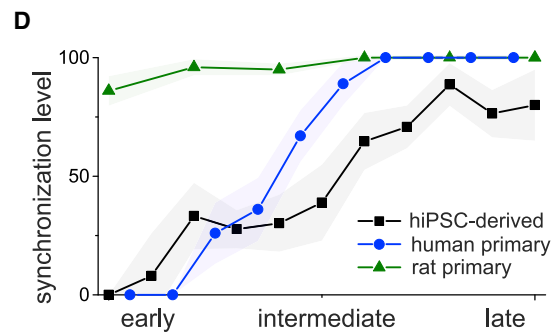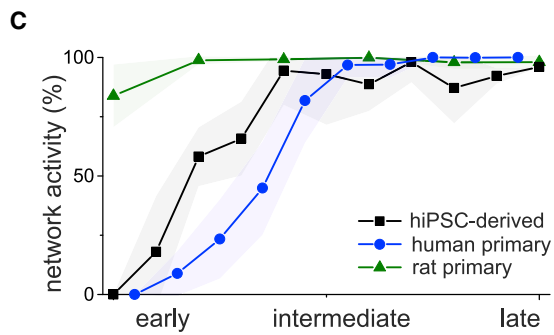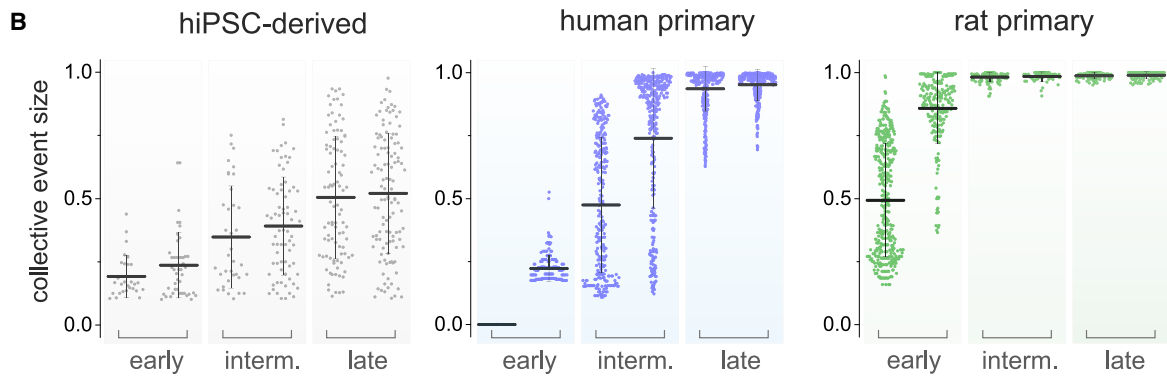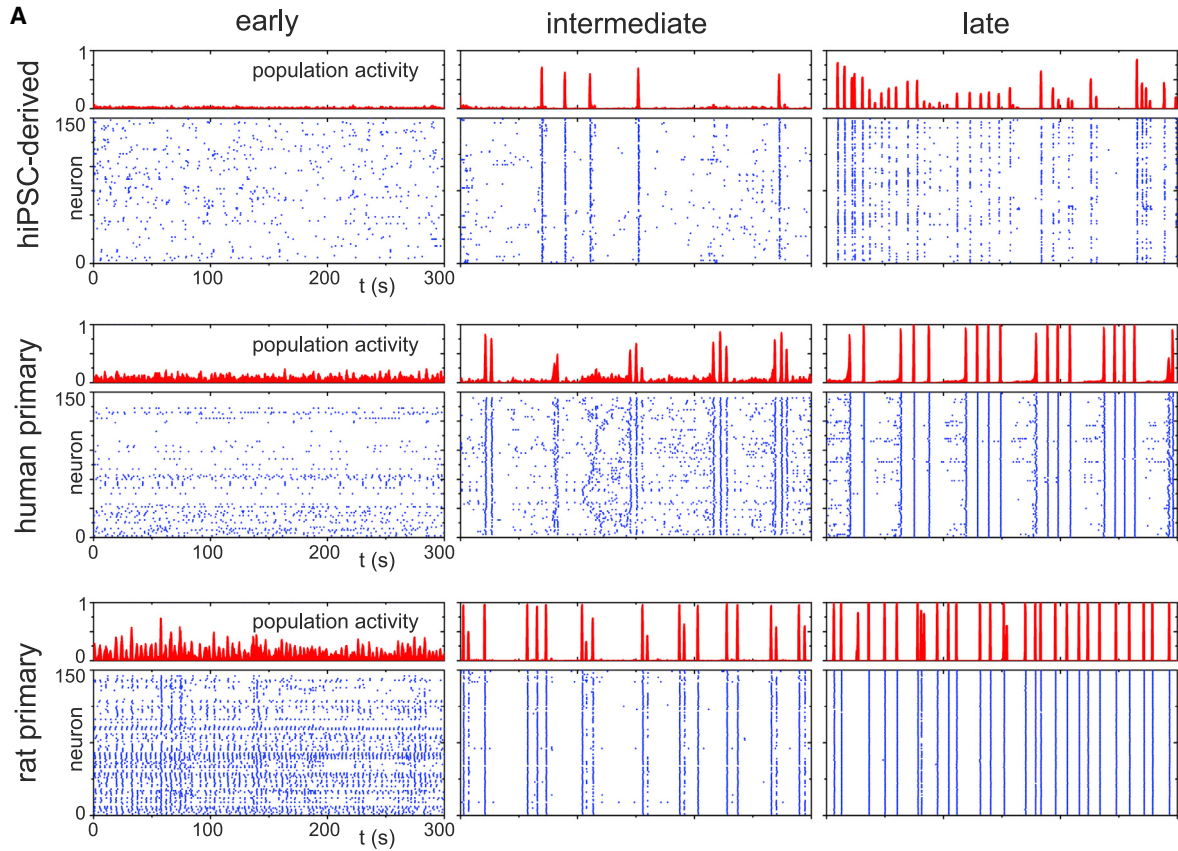
(legend on next page)

indicating that neuronal coactivations encompassed a different number of neurons. Human primary cultures showed a very similar trend (Figure 3A, middle panel), with sporadic activity during early development that gradually switched to synchronous-dominated dynamics, but with less variability in population strength at mature timepoints. By contrast, rat primary cultures showed strong collective activity from the early stages of network development, and fully synchronous behavior emerged almost immediately (Figure 3A, bottom panel), involving nearly all monitored neurons and lacking the smooth transition featuring both sporadic and coordinated activity seen in the other cases.

The analysis of the distribution of collective event sizes (Figure 3B) provided further insight into the maturation process of the generated neuronal networks. In the distributions, two representative examples from different batches of each culture type were plotted, and their structure was compared along development. While hiPSC-derived and human primary cultures (Figure 3B, left and middle, respectively) steadily grew in event size, the transition from scattered activity to whole synchronization was very sharp for rat primary cultures, and no richness in the distribution was observed at either intermediate or late levels of development. This again emphasizes the strong dynamic rigidity of rat primary cultures.

We next used a set of descriptors to compare the evolution of the different culture types. Network activity (Figure 3C) was defined as the percentage of neurons active relative to all detected neurons in the field of view. To make the different conditions comparable, we interpolated the data to have about 6–10 points per condition, which were averaged out among six repetitions per condition (see supplemental methods). The first point in the sequence corresponded to the observation of widespread GCaMP6s expression in the culture, and the last one corresponded to a stable culture, i.e., that its overall activity did not evolve further within 2 days. Comparison of the network activity in the three culture types showed that, while in rat primary cultures practically all monitored neurons were active from the very beginning with small variations among repetitions, in hiPSC-derived and human primary cultures, activity slowly emerged and steadily en-

compassed a larger number of monitored neurons until practically all neurons were always active. The smooth transition from no activity to a strong one is interesting and makes these cultures ideal to study the gradual formation of neuronal circuits along with development.

Similarly, the synchronization level measures the percentage of collective events that encompassed at least 25% of the network relative to all observed collective events among the recordings. The study of this descriptor during network development underlined that rat primary cultures exhibited high levels of synchronization in the early stages, as most of the collective events were higher than 25% (Figure 3D). In contrast, hiPSC-derived and human primary cultures showed a gradual increase in the synchronization level along time, reflecting their richness in the distribution of event sizes. However, while hiPSC-derived cultures did not reach 100% synchronization due to the presence of small collective events (<25% network) at mature stages, human primary cultures reached 100% synchronization (Figure 3B).

Analysis of neural dynamic interactions unravels a functional organization typical of human-derived cultures

Given the differences in dynamic behavior across culture types, we next investigated whether these differences revealed characteristic features in the functional organization of the cultures. For that, we used the raster plots to compute the functional connectivity between neuronal pairs (see experimental procedures), which captures the likelihood of neurons to exchange information with one another. To provide an overview of the differences between cultures, we first considered the functional characteristics at the late stages of development and generated adjacency connectivity matrices and network connectivity maps for the three culture types explored. Representative matrices and maps are shown in Figure 4A, top and bottom panel respectively. In the connectivity matrices, black dots indicate effective connections between neuronal pairs, where the same neurons (from 0 to 150) are represented in both axes. The order of those neurons in the matrices was arranged to highlight the presence of functional communities along the diagonal (color boxes), which conceptually

Figure 3. Network activity along with the development
(A) Raster plots of activity for early, intermediate, and late stages of development for the three culture conditions. Each raster plot is accompanied by the population activity profile on top, in which sharp peaks mark strong synchronous activity.
(B) Distribution of collective activity events. Each dot conceptually corresponds to a peak in the population activity profile of (A). The black line indicates the mean of the distributions. Each distribution is built by pooling together six different culture repetitions on the same measurement day. For hiPSC-derived and human primary cultures, data includes the immediately adjacent recording day.
(C) Evolution of network activity along with development.
(D) Synchronization level, measured by counting the fraction of collective activity events that encompass at least 25% of the network. Data in (C–D) are based on the statistics of six different repetitions per culture type. Color shadings are the SD of the mean.
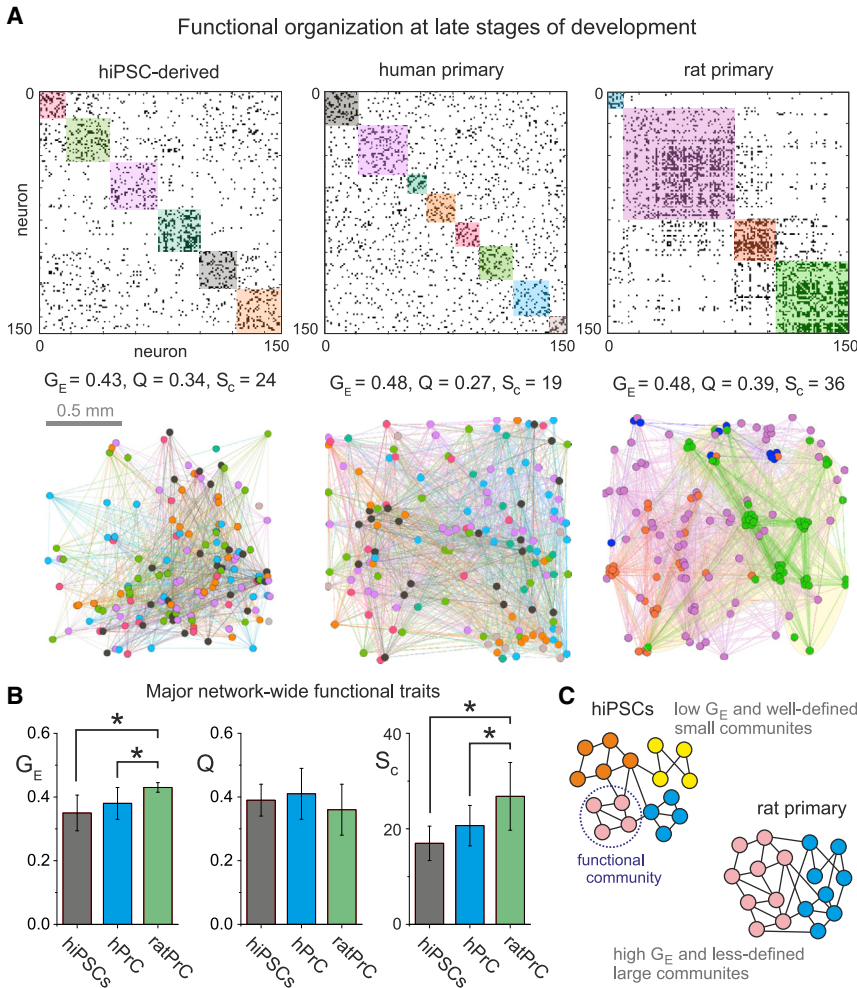
A Functional organization at late stages of development

hiPSC-derived | human primary | rat primary

$G_E = 0.43$, $Q = 0.34$, $S_c = 24$ | $G_E = 0.48$, $Q = 0.27$, $S_c = 19$ | $G_E = 0.48$, $Q = 0.39$, $S_c = 36$

0.5 mm

B Major network-wide functional traits

G_E | Q | S_c

hiPSCs / hPrC / ratPrC

C hiPSCs — low G_E and well-defined small communites

functional community

rat primary

high G_E and less-defined large communites

Figure 4. Effective connectivity analysis and functional organization
(A) Top, adjacency connectivity matrices for the late stages of development shown in Figure 3A. Black dots are effective connections, and color boxes are functional communities. Bottom, corresponding network connectivity maps, illustrating that connections and functional communities extended throughout the entire field of view and are highly interwoven. The spatial extent of a functional community is shown for the rat primary culture as a yellow patch.
(B) Comparison of major network properties (high global efficiency G_E, community statistic Q, and community sizes S_c) for the three culture conditions.
(C) Sketch comparing the contrasting behavior at a network level between hiPSC-derived and rat primary cultures, with the latter exhibiting a higher overall integration.
Data in (B) are averaged over six different repetitions per culture type. *p < 0.05 (Student's t test).

indicate groups of neurons that tend to interact more strongly within their community than with the rest of the network. Thus, black dots inside the color boxes indicate intra-community connections, while those outside indicate inter-community connections.

Analysis of the connectivity matrices showed that, in all three models, there was an abundance of functional connections both inside and outside the communities, which denotes that the neurons easily communicate on a global scale. The capacity for network-wide communication was captured by the global efficiency G_E, and that was similar for the three types of cultures (around $G_E \simeq 0.46$, Figure 4A middle line). This global communication arose from the strong synchronization of neurons during bursting episodes (Figure 3A, right panels), a dynamical trait that was shared among cultures in the different models. However, this similar global communication contrasts with the structure of the communities, whose size S_C was about 50% smaller for hiPSC-derived and human primary cultures

compared with rat primary cultures (Figure 4A, middle line). The reason for this difference is the richer dynamics of hiPSC-derived and human primary cultures, in which sporadic, weakly correlated activity is combined with network bursts, favoring a richer repertoire of communication among neurons. At the same time, network-wide synchronous activity was always present in the three culture types, showing that the communities were well bound to one another. This was captured by the community statistic Q, which conceptually reflects the tendency of a network to form distinct communities. The larger Q, the stronger the segregation of the network. Moderate values of Q, in the range $0.27 - 0.39$ for the examples shown (Figure 4A, middle line), indicate that communities were present, but that they did not dominate the structure of the network.

The connectivity maps (Figure 4A, bottom) provided insight into the spatial extent of the functional communities. Neurons and connections in the maps are colored according to their community. In general, illustrating
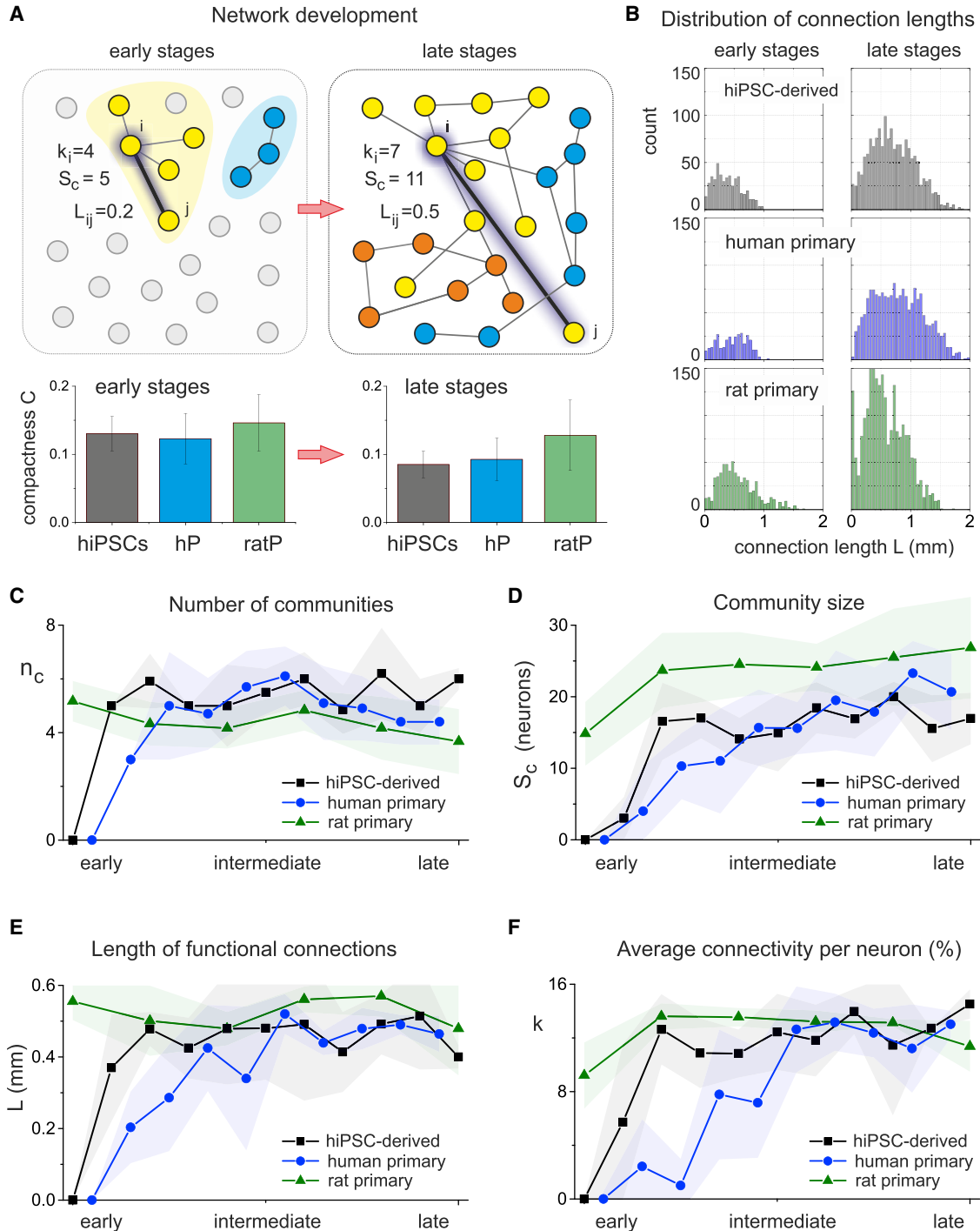
Figure 5. Evolution of network functional properties along with the development

(A) Sketch showing general connectivity properties and their change upon maturation. At early stages, the neuron indicated in blue connects with four others, communicates at a short-range, and belongs to a community formed by five nearby neurons. At late stages, the same neuron is more connected and communicates with long-range neurons, shaping a spatially extended bigger community that is blended with other communities. The bar plots at the bottom compare the compactness *C* at early and late stages for the three culture conditions.

(legend continued on next page)

that connections and functional communities extended throughout the entire field of view, and the communities were spatially blended, which again is a consequence of network-wide communication induced by bursting. It is interesting to highlight, however, that communities in rat primary cultures tended to be more spatially compact. This is indicated by a yellow contour in one of the communities (formed by the green-colored community). The reason for this spatial segregation is the preferential connectivity and communication of the neurons with their neighbors in this type of culture.

To obtain further insight into distinct features among the three conditions and address the consistency of the results, we averaged the descriptors of the functional organization of the networks (G_E, Q, and S_C) including six repetitions per condition (Figure 4B). Interestingly, we observed that the global efficiency G_E and the community size S_C were significantly larger for rat primary compared with hiPSC-derived and human primary cultures, which is due to the systematic presence of stronger bursting for rat cultures. Human primary cultures fell in between the previous conditions, which is possibly due to the higher presence of sporadic activity events compared with rat primary cultures. The community statistic Q was similar among conditions on average, although there was a tendency to be smaller for rat primary cultures, indicating that the functional communities were more interconnected. For completeness, the evolution of G_E and Q along development is provided in Figure S2. Rat primary cultures were locked since the very beginning in a synchronous state that functionally corresponds to a highly integrated network, procuring practically constant G_E and Q values that were typically above (for G_E) or below (Q) those of hiPSC-derived and human primary cultures. These latter cultures, in turn, also exhibited gradual changes in G_E and Q as they matured. Finally, the community size S_C was significantly higher for rat primary cultures, although variability was high. The evolution of S_C along development is depicted later in Figure 5. Both the lower Q and higher S_C for rat primary cultures are a consequence of their overall stronger synchronization during activity. A network sketch summarizing the key differences between hiPSC-derived and rat primary cultures is provided in Figure 4C. The aim of the sketch is to emphasize the global trend that hiPSC-derived cultures shaped a functionally segregated network, with relatively small G_E and S_C as well as better defined communities, while rat primary cultures tended to be overall more

integrated. Human primary cultures fell in between the two cases shown.

The evolution of network functional properties showed differences between human and rat cultures

To deepen further into the functional connectivity analysis, we investigated other network traits and their evolution along with the development of the neuronal networks in the different conditions, including the connectivity k_i of a given neuron i and the length of an effective connection L_{ij} from neuron i to j, as sketched in Figure 5A. The sketch aims at illustrating that neurons tend to functionally interact within a neighborhood at the early stages of development, with an average low connectivity k and short connections L, and that these properties gradually grow along with development, with L reaching the size of the field of view at late stages. Neurons that are not sufficiently mature to show activity or that do not significantly communicate with others are illustrated in gray. The communities are relatively small in size (S_C) at early stages to gradually grow, with communities typically extending the monitored area and crossing one another. The functional communities (depicted with different colors in the sketch) also start small and gradually grow, both in size and spatial coverage.

It is worth pointing out that functional communities were typically strongly interwoven in the studied cultures. This can be quantified by the spatial compactness C of communities (see supplemental information), whose values vary between 0, when the neurons of a community are scattered without any characteristic shape, and 1, when they are physically close to one another and shape a compact, circle-like spot. The analysis of the network maps provided in Figure 4A indicated that functional communities, both at early and late stages of development, had very low compactness around $C \simeq 0.1$ (bottom bar plots in Figure 5A); i.e., the communities were well spatially mixed. However, the compactness at early stages was about 40% higher than at late stages, which we hypothesize is due to the initial formation of functional communities in small neighborhoods (as in the sketch of Figure 5A). To verify this hypothesis, we computed the distribution of functional connection lengths L for the representative experiments of Figure 4A, and we compared early and late developmental stages (Figure 5B). The distributions show that, at early stages, functional connections rarely extend beyond 1 mm (i.e., communication is more localized in neighborhoods), while at late stages the entire field of view of 2 mm is reachable. We

(B) Histograms of effective connectivity distances for the representative experiments shown in Figure 4A and comparing early and late developmental stages. Aggregation in rat primary cultures imprints a peak in the histogram at short-range scales.

(C–F) Evolution of different network properties. Data in these panels are based on the statistics of six different repetitions per culture type, and color shadings are the SD of the mean.

note that the distributions of connection lengths at intermediate and late stages were very similar due to the presence of network-wide bursting in both cases, leading to abundant whole-network communication. We also note that, for hiPSC-derived and human primary cultures at late stages, the distributions in Figure 5B are broad, and both short- and long-range connections are prominent, with distribution means around $L \simeq 0.7$ mm for both cases. The shape of the distribution is slightly different for rat primary cultures, with approximately the same mean but with peaks at $L \simeq 0.4$ mm and $L \simeq 1$ due to the already mentioned preferential connectivity and communication of the neurons with their neighbors in this condition.

The evolution of the average number of communities n_c along development (Figure 5C) showed that rat primary cultures already exhibited a considerable number of communities (around 5) since early stages, a value that slowly decreased to 4 as synchronization strengthened. In contrast, in hiPSC-derived and human primary cultures, n_c steadily grew and was typically larger than rat cultures due to the weaker overall synchronization, although for human cultures there was a tendency to gradually approach the behavior of rat cultures at the latest stages of development, possibly because some of the repetitions in human cultures had similar levels of strong bursting as rat primary cultures. The evolution of the community size S_c (Figure 5D) abruptly increased for rat primary cultures to encompass about 25 neurons on average along the rest of development. In contrast, for hiPSC-derived cultures, we observed a fast increase, and S_c remained approximately constant at around 17 neurons, while for human primary cultures there was a gradual increase in S_c, remaining in between hiPSC-derived and rat primary cultures at the last stages of development.

The average effective connectivity length L (Figure 5E) was high since early development in rat primary cultures and afterward remained practically constant. This is somehow expected since these cultures were already bursting since almost the first day of measurements, and therefore network-wide communication was expected. We also observed a gradual increase in L for hiPSC-derived and human primary cultures, but the increase was both due to the presence of new active neurons and the strengthening of network-wide communication. Particularly for human primary cultures, we hypothesize that the decrease and sudden jump of L at intermediate stages of development is probably due to a scenario in which all cells were active, but the network transited from scattered activity to bursting behavior. Similarly, the average connectivity k (Figure 5F) directly jumped to high values for rat primary cultures and stayed practically constant, while k gradually grew for hiPSC-derived and human primary cultures. The values of k were upper bounded by the number of active neurons in the network. For N active neurons, a neuron can connect to at most $N–1$ other neurons. Thus, k captures well the formation of new connections in the network as more neurons become active. This formation seems more gradual in human primary cultures than in hiPSC-derived ones. However, for the latter, we observed strong variability across repetitions for similar time points, with some cultures exhibiting few active neurons, while others were starting to display synchronous behavior.

DISCUSSION

Here we presented a set of tools that served to assess the progression of neuronal network maturation in cell cultures and their application to quantitively compare three neuronal culture models, namely hiPSC-derived, human primary, and rat primary cultures. Using the genetically encoded calcium indicator GCaMP6s, we showed, for the first time to our knowledge, continuous temporal monitoring of neural activity of the same group of neurons, with single-cell resolution, throughout the emergence of activity and the process of network formation in these three models of interest.

In all three culture types, functional neuronal networks reached high levels of complexity characterized by abundant spontaneous activity and rich functional organization that comprised communication within small communities and whole-network interactions. Although previous studies have pointed out the capacity of neuronal assemblies to self-organize and become functionally rich (Poli et al., 2015; Schroeter et al., 2015), a comparative approach of functional network development between different culture types under the same conditions was missing, particularly when inquiring whether these cultures shaped unique characteristics that could be ascribed to specific species or cell origin. Our tracking protocol showed that the emergence of the complex functional organization was gradual for hiPSC-derived and human primary cultures but abrupt for rat primary cultures. Previous works have shown prolonged maturation and single-cell integration times for human neurons compared with rodent ones after transplantation in a mouse model (Linaro et al., 2019).

It is noteworthy that rat primary cultures were strongly locked in a synchronous dynamic behavior since the detection of activity by GCaMP6s. This strong synchronization, in turn, led to functional networks that were excessively integrated, a condition that is considered pathological when compared with healthy brain-like behavior (Deco et al., 2015). A richer repertoire of activity and functionality in rat primary cultures could be favored by imprinting modular characteristics in the network, for instance through strong aggregation (Teller et al., 2014;

Okujeni and Egert, 2019; Tibau et al., 2020) or fine-tuned neuro-engineering (Yamamoto et al., 2018; Montalà-Flaquer et al., 2022). By contrast, hiPSC-derived cultures exhibited a broad repertoire of activity patterns (functional segregation), and the synchronous-like behavior present at late stages did not dominate network dynamics. Intuitively, some features and pathophysiological aspects specific to the human brain cannot be naturally expressed by animal models and may explain the conspicuous dissimilarities encountered between hiPSC-derived and rat primary cultured neuronal networks. Despite the inherent differences between neuronal cultures and *in vivo* circuits or brain slices, the richer behavior of hiPSC-derived cortical cultures resembles that observed in cortical slices and *in vivo* recordings, which has special relevance in the procedural design and implementation of new brain-inspired technologies, such as brain-on-chip approaches (Amirifar et al., 2022), which indeed procure more realistic extracellular scenarios using human cell lines while maintaining the environmental control of *in vitro* studies.

Our tracking protocol is similar to a previous study (Hyvärinen et al., 2019) that used multielectrode arrays instead of calcium imaging to follow in parallel the development of hiPSC-derived and rat primary cultures. Despite differences in culturing protocols and tracking technology, they also reported richer dynamic and functional characteristics in hiPSC-derived cultures. Moreover, in our study, we incorporated human primary cultures as an additional model to address whether the observed differences were intrinsic features peculiar to human cells. The scarcity of original human tissue and the underlying ethical debate hinders the use of embryo human neurons in research (Rossant and Tam, 2021). Thus, the use of these cells with the same protocol provides an invaluable opportunity to also measure the extent to which hiPSC-derived cultures resemble primary human neuronal networks. Interestingly, our work showed that human primary cultures share most functional traits with hiPSC-derived cultures, despite some small similarities with rat primary cultures, particularly at late stages of development, such as a strong bursting and network-wide integration.

It is important to highlight that one of the most evident morphological differences observed between human- and rat-derived cultures is not related to neurons, but rather the astrocytes. These important cellular components are known to be crucial for the correct generation and maturation of neuronal networks, not only during brain development but also in *in vitro* models (Muratore et al., 2014; Prè et al., 2014; Schutte et al., 2018; Burke et al., 2020). Moreover, this maturation process is dependent on cell-to-cell contact, since it was shown that an astrocyte-conditioned medium was not sufficient to increase synaptic activity in human embryonic stem cell-derived neuronal cultures

(Johnson et al., 2007). Although most of the previous studies using co-cultures of human neuronal cultures were carried out with mouse astrocytes, our results may suggest that human astrocytes could be one of the players involved in the richer dynamics observed in the human-derived cultures.

Our results show different phases in the generation and maturation of neuronal networks *in vitro*, especially when using human cells. It was evident from the raster plots that the frequency of neuronal activity in the cultures increased rapidly after the early stages, arriving at a maximum level during the intermediate one, to later fluctuate around an average value toward the end of the tracking protocol, indicating that cultures did not evolve further. This behavior was previously observed in a similar study (Kirwan et al., 2015) and resembles the one found in the developing cerebral cortex *in vivo*, demonstrating the utility of *in vitro* systems based on human cells for mechanistic studies.

It is well known that both *in vitro* and *in vivo* cortical cells are sequentially generated from neural progenitors, with the neurons characteristic of deeper layers of the cortex (TBR1-positive) appearing earlier and the ones from more superficial layers (CDP/SATB2-positive) originating afterward (Gaspard et al., 2008). Based on the characterization of our cultures, with the majority of the neurons expressing TBR1 and just a few being positive for SATB2 or CDP (data not shown), this sequential generation was most likely influencing the functional traits observed in our results. However, further studies will be needed to clarify the relation between cortical cells formation and network dynamics and functionality.

Our work emphasizes the strong differences between hiPSC-derived and rodent primary cultures along with the development and the in-between features of human primary cultures. This is important also for the use of *in vitro* preparations in the study of neurological disorders. A recent work (Carola et al., 2021) used hiPSC-derived cultures to detect early functional alterations in networks affected by Parkinson disease. The default balance between integration and segregation of hiPSC-derived cultures was central in the work by Carola et al. to uncover such an over-synchronous anomaly. This kind of study will benefit from our findings by accurately locating malfunction features specific to human's rich connectivity dynamics.

In conclusion, our work shows that hiPSC-derived cultures are a better culture model for their gradual maturation, availability, and more varied spatiotemporal activity, closer to the traits observed *in vivo*. Given the relevance of culture models in medicine and the current challenges in translation to clinical studies, these network characteristics and functional development fingerprints may be

crucial for several lines of research involved in neuronal networks: to uncover early signs of degeneration in developing networks, to better predict outcomes from preclinical drug discovery, to tailor brain-inspired engineered and *in silico* models, to enhance precision medicine efficacy, and to understand functional deficits in complex maturing systems.

EXPERIMENTAL PROCEDURES

Resource availability

Corresponding author

Correspondence: eestevez@lst.tfo.upm.es and daniel.tornero@ub.edu

Materials availability

All non-commercially available materials used in this work will be available upon request to the authors.

Data and code availability

Most analyses were carried out with the Netcal software, available here: https://zenodo.org/record/1119026#.Y2owZHbMJjU. Additional analyses were conducted using home-made software in MATLAB, and they are available upon request to the authors.

Cell culture

Human iPSC-derived neuronal cultures

Human iPSC-derived cortical NPCs from healthy male newborns (Axol Bioscience) were grown in Neuronal Expansion Media (Axol Bioscience), supplemented with 1:100 penicillin-streptomycin (Gibco) and 1:50 B27 (Gibco). For differentiation into cortical neurons, cells were detached with Unlock Solution (Axol Bioscience) and transferred to bottom-glass-coated Petri dishes (Ibidi) at a final density of 200–400 neurons/mm^2 (coating protocol detailed in supplemental information). This time point was set as DD0. Media was switched at DD1 to Neural Differentiation XF Media (Axol Bioscience) and finally at DD4 to BrainPhys (Stem Cell Technologies), supplemented with 1:50 B27 without retinoic acid (Gibco) and 1:100 penicillin-streptomycin, which was renewed every 3–4 days onward. 1 week after starting differentiation (DD7), cells were infected with the AAV containing the fluorescence indicator GCaMP6s under the control of Syn-I promoter (1 μL/mL).

Rat primary cultures

For cultures of rat embryonic cells (E18–E19) from the cortex, all procedures were approved by the Animal Experimentation Ethics Committee (CEEA) of the University of Barcelona, under order DMAH-5461, in accordance with the regulations of the Generalitat de Catalunya (Spain). Briefly, dissection was carried out in ice-cold L-15 medium (Gibco), enriched with 0.6% glucose and 0.5% gentamicin (Sigma-Aldrich). The extracted brain cortices were isolated from the meninges, transferred to cell media, and dissociated mechanically by pipetting. The final suspension was plated on the bottom-glass-coated Petri dishes (Ibidi), corresponding to DD0. The density after seeding was 200–400 neurons/mm^2. 2 days after plating (DD2), cells were infected with AAV-GCaMP6s (1 μL/mL). At DD5, cultures were treated with 0.5% FUDR for 3 days to restrict glial proliferation. Afterward, cells were maintained with periodic medium renewal every 3 days, using BrainPhys, supplemented with 1:50 B27 without retinoic acid and 1:100 penicillin-streptomycin.

Human primary cultures

Cortical tissue from dead, aborted human fetuses at 7–9 weeks post-conception was obtained from Lund and Malmö University Hospitals according to the guidelines approved by Lund/Malmö Ethical Committee. The tissue was micro-dissected under a stereomicroscope (Leica, Germany) and frozen in Stem Cell Banker (AMSBIO). At the moment of culture preparation, frozen tissue was resuspended in BrainPhys Media and dissociated mechanically by pipetting. Then, the cell suspension was diluted with BrainPhys supplemented with 1:50 B27 without retinoic acid and 1:100 penicillin-streptomycin and plated on bottom-glass-coated Petri dishes (Ibidi), reaching a final density of 200–400 neurons/mm^2. 1 week after plating (DD7), cells were infected with AAV-GCaMP6s (1 μL/mL).

Immunocytochemistry

Immunostaining of cultures was carried out as previously described (Tornero et al., 2013), with minor changes as detailed in supplemental information.

Intracellular calcium fluorescence imaging

Neuronal cultures were plated on grid-labeled Petri dishes to allow monitorization of the same region within a culture along with the tracking protocol, thus ensuring that inferred development features corresponded to the same cells. Neuronal network activity was monitored using the genetically encoded calcium fluorescence indicator GCaMP6s. Recordings were carried out every 3 days, at 37°C, and with a duration of 10 min at 33 images/s. Extensive details are provided in the supplemental information.

Data analysis

Recorded movies of calcium fluorescence activity were analyzed with the software NETCAL (www.itsnetcal.com) (Fernández-García et al., 2020) in combination with other custom-made packages, providing the raster plots of spontaneous neuronal activity. For clarity of visualization, data in raster plots was reduced to 150 neurons along 5 min of activity. The "population activity" was next computed from the raster plots to quantify the tendency of neurons in the network to activate collectively in a short time window. The strength of collective activity was denoted A and varied between 0 (no activity) and 1 (network-wide activation), and all detected collective events A across comparable time points and repetitions were pooled together to build the distribution of collective event sizes. The "synchronization index" was then introduced to determine whether the activity was dominated by ensemble activity (few neurons) or network-wide events, and it was defined as the percentage of collective event sizes encompassing at least 25% of neurons in the network. Extensive details of data analysis are provided in the supplemental information.

Functional connectivity

Generalized transfer entropy (GTE) (Stetter et al., 2012; Ludl and Soriano, 2020; Tibau et al., 2020) was used to compute causal relationships among pairs of neurons, and it followed the same procedure and analysis tools as described in Ludl and Soriano (2020). All details of effective connectivity inference are provided

in the supplemental information and in Ludl and Soriano (2020). GTE pipeline provided binary and directed connectivity matrices were "1" and "0" indicated, respectively, the presence or absence of a connection. Matrices were visualized in the form of network maps with Gephi (Bastian et al., 2009). Additionally, to avoid artifacts when comparing network characteristics across culture types, all studied functional networks were reduced to $N = 100$ randomly chosen neurons, so all had the same size. For illustrative purposes, the networks in Figure 4A were rendered with 150 neurons, but all statistical analyses that include network properties are carried out with 100 neurons.

Network properties

Functional connectivity matrices were analyzed using the "Brain Connectivity Toolbox" (Rubinov and Sporns, 2010) to quantify the topological organization of the studied cultures. Five main network properties were used and are described in detail in the supplemental information and in Ludl and Soriano (2020) and Montalà-Flaquer et al. (2022). Briefly, these properties covered the following characteristics. The "average connectivity" k measured the percentage of functional connections that a neuron establishes with any other neuron in the network. A value of $k = 100\%$ would mean that a neuron connects with all the others. The "global efficiency" G_E accounted for the capacity of neurons to exchange information across the entire network and varied between 0 (neurons disconnected) and 1 (all neurons reachable through just one connection). Large values of G_E reflected neuronal networks that were highly integrated, while low values indicated strong segregation. The "community statistic" Q described the tendency of neurons to form functional communities, i.e., groups of neurons that were more connected within their group than with neurons in other groups. Q ranged between 0 (the entire network shaped a unique community) and 1 (each neuron is an isolated community). Values of $Q \geq 0.3$ indicated the existence of clear communities in the network and were highlighted as colored boxes in the representation of adjacency matrices. The "number of communities" n_c was defined as the number of detected communities containing at least five neurons. The "community size" S_c was the corresponding average number of neurons per community. The "length of functional connections" L measured Euclidean distance between any pair of effectively connected neurons. L reflected the range at which neurons could communicate to one another. The "spatial compactness of functional communities" C referred to the property of objects to exhibit a minimum perimeter P for a given area S, and it was mathematically measured through the Polsby-Popper test, $C = 4\pi S/P^2$, with $C = 0$ for a lack of compactness, e.g., randomly scattered spots, and 1 for a circle, the most compact shape.

Statistical analysis

All statistical analysis was performed with Origin 9.0 and MATLAB 2018b. Unless otherwise stated, data are plotted as the mean ± SD of the mean. All data points were averaged over at least six independent repetitions unless specified.

SUPPLEMENTAL INFORMATION

Supplemental information can be found online at https://doi.org/10.1016/j.stemcr.2022.11.014.

REFERENCES

Amirifar, L., Shamloo, A., Nasiri, R., de Barros, N.R., Wang, Z.Z., Unluturk, B.D., Libanori, A., Ievglevskyi, O., Diltemiz, S.E., Sances, S., et al. (2022). Brain-on-a-chip: recent advances in design and techniques for microfluidic models of the brain in health and disease. Biomaterials 285, 121531.

Bastian, M., Heymann, S., and Jacomy, M. (2009). Gephi: An Open Source Software for Exploring and Manipulating Networks (International AAAI Conference on Weblogs and Social Media).

Bellin, M., Marchetto, M.C., Gage, F.H., and Mummery, C.L. (2012). Induced pluripotent stem cells: the new patient? Nat. Rev. Mol. Cell Biol. 13, 713–726.

Burke, E.E., Chenoweth, J.G., Shin, J.H., Collado-Torres, L., Kim, S.K., Micali, N., Wang, Y., Colantuoni, C., Straub, R.E., Hoeppner, D.J., et al. (2020). Dissecting transcriptomic signatures of neuronal differentiation and maturation using iPSCs. Nat. Commun. 11, 1–14. https://doi.org/10.1038/s41467-019-14266-z.

Carola, G., Malagarriga, D., Calatayud, C., Pons-Espinal, M., Blasco-Agell, L., Richaud-Patin, Y., Fernandez-Carasa, I., Baruffi, V., Beltramone, S., Molina, E., et al. (2021). Parkinson's disease patient-specific neuronal networks carrying the LRRK2 G2019S mutation unveil early functional alterations that predate neurodegeneration. NPJ Parkinsons Dis. 7, 55.

Chiappalone, M., Bove, M., Vato, A., Tedesco, M., and Martinoia, S. (2006). Dissociated cortical networks show spontaneously correlated activity patterns during in vitro development. Brain Res. 1093, 41–53.

Deco, G., Tononi, G., Boly, M., and Kringelbach, M.L. (2015). Rethinking segregation and integration: contributions of whole-brain modelling. Nat. Rev. Neurosci. 16, 430–439.

Dingle, Y.-T.L., Liaudanskaya, V., Finnegan, L.T., Berlind, K.C., Mizzoni, C., Georgakoudi, I., Nieland, T.J.F., and Kaplan, D.L. (2020). Functional characterization of three-dimensional cortical cultures for in vitro modeling of brain networks. iScience 23, 101434.

Eytan, D., and Marom, S. (2006). Dynamics and effective topology underlying synchronization in networks of cortical neurons. J. Neurosci. 26, 8465–8476.

Fernández-García, S., Orlandi, J.G., García-Díaz Barriga, G.A., Rodríguez, M.J., Masana, M., Soriano, J., and Alberch, J. (2020). Deficits in coordinated neuronal activity and network topology are striatal hallmarks in Huntington's disease. BMC Biol. 18, 58.

Gaspard, N., Bouschet, T., Hourez, R., Dimidschstein, J., Naeije, G., van den Ameele, J., Espuny-Camacho, I., Herpoel, A., Passante, L., Schiffmann, S.N., et al. (2008). An intrinsic mechanism of cortico-genesis from embryonic stem cells. Nature 455, 351–357.

Hyvärinen, T., Hyysalo, A., Kapucu, F.E., Aarnos, L., Vinogradov, A., Eglen, S.J., Ylä-Outinen, L., and Narkilahti, S. (2019). Functional characterization of human pluripotent stem cell-derived cortical networks differentiated on laminin-521 substrate: comparison to rat cortical cultures. Sci. Rep. 9, 17125.

Inoue, H., Nagata, N., Kurokawa, H., and Yamanaka, S. (2014). iPS cells: a game changer for future medicine. EMBO J. 33, 409–417.

Johnson, M.A., Weick, J.P., Pearce, R.A., and Zhang, S.C. (2007). Functional neural development from human embryonic stem cells: accelerated synaptic activity via astrocyte coculture. J. Neurosci. 27, 3069–3077.

Kirwan, P., Turner-Bridger, B., Peter, M., Momoh, A., Arambepola, D., Robinson, H.P.C., and Livesey, F.J. (2015). Development and function of human cerebral cortex neural networks from pluripotent stem cells in vitro. Development (Camb.) 142, 3178–3187.

Koroleva, A., Deiwick, A., El-Tamer, A., Koch, L., Shi, Y., Estévez-Priego, E., Ludl, A.A., Soriano, J., Guseva, D., Ponimaskin, E., and Chichkov, B. (2021). In vitro development of human iPSC-derived functional neuronal networks on laser-fabricated 3D scaffolds. ACS Appl. Mater. Interfaces 13, 7839–7853.

Linaro, D., Vermaercke, B., Iwata, R., Ramaswamy, A., Libé-Philip-pot, B., Boubakar, L., Davis, B.A., Wierda, K., Davie, K., Poova-thingal, S., et al. (2019). Xenotransplanted human cortical neurons reveal species-specific development and functional integration into mouse visual circuits. Neuron 104, 972–986.e6.

Ludl, A.-A., and Soriano, J. (2020). Impact of physical obstacles on the structural and effective connectivity of in silico neuronal circuits. Front. Comput. Neurosci. 14, 77.

Montalà-Flaquer, M., López-León, C.F., Tornero, D., Fardet, T., Monceau, P., Bottani, S., and Soriano, J. (2022). Rich dynamics and functional organization on topographically designed neuronal networks in vitro. Preprint at bioRxiv. https://doi.org/10.1101/2022.09.28.509646.

Muratore, C.R., Srikanth, P., Callahan, D.G., and Young-Pearse, T.L. (2014). Comparison and optimization of hiPSC forebrain cortical differentiation protocols. PLoS One 9, e105807.

Okujeni, S., and Egert, U. (2019). Self-organization of modular network architecture by activity-dependent neuronal migration and outgrowth. Elife 8, e47996.

Orlandi, J.G., Soriano, J., Alvarez-Lacalle, E., Teller, S., and Casa-demunt, J. (2013). Noise focusing and the emergence of coherent activity in neuronal cultures. Nat. Phys. 9, 582–590.

Park, I.-H., Arora, N., Huo, H., Maherali, N., Ahfeldt, T., Shima-mura, A., Lensch, M.W., Cowan, C., Hochedlinger, K., and Daley, G.Q. (2008). Disease-specific induced pluripotent stem cells. Cell 134, 877–886.

Pasquale, V., Massobrio, P., Bologna, L.L., Chiappalone, M., and Martinoia, S. (2008). Self-organization and neuronal avalanches in networks of dissociated cortical neurons. Neuroscience 153, 1354–1369.

Petros, T.J., Tyson, J.A., and Anderson, S.A. (2011). Pluripotent stem cells for the study of CNS development. Front. Mol. Neurosci. 4, 1–12.

Poli, D., Pastore, V.P., and Massobrio, P. (2015). Functional con-nectivity in in vitro neuronal assemblies. Front. Neural Circuits 9, 57.

Prè, D., Nestor, M.W., Sproul, A.A., Jacob, S., Koppensteiner, P., Chinchalongporn, V., Zimmer, M., Yamamoto, A., Noggle, S.A., and Arancio, O. (2014). A time course analysis of the electrophysiological properties of neurons differentiated from hu-man induced pluripotent stem cells (iPSCs). PLoS One 9, e103418.

Rossant, J., and Tam, P.P.L. (2021). Opportunities and challenges with stem cell-based embryo models. Stem Cell Rep. 16, 1031–1038.

Rubinov, M., and Sporns, O. (2010). Complex network measures of brain connectivity: uses and interpretations. Neuroimage 52, 1059–1069.

Schroeter, M.S., Charlesworth, P., Kitzbichler, M.G., Paulsen, O., and Bullmore, E.T. (2015). Emergence of rich-club topology and co-ordinated dynamics in development of hippocampal functional networks in vitro. J. Neurosci. 35, 5459–5470.

Schutte, R.J., Xie, Y., Ng, N.N., Figueroa, P., Pham, A.T., and O'Dowd, D.K. (2018). Astrocyte-enriched feeder layers from cryo-preserved cells support differentiation of spontaneously active networks of human iPSC-derived neurons. J. Neurosci. Methods 294, 91–101.

Shi, Y., Kirwan, P., and Livesey, F.J. (2012). Directed differentia-tion of human pluripotent stem cells to cerebral cortex neurons and neural networks. Nat. Protoc. 7, 1836–1846.

Stetter, O., Battaglia, D., Soriano, J., and Geisel, T. (2012). Model-free reconstruction of excitatory neuronal connectivity from calcium imaging signals. PLoS Comput. Biol. 8, e1002653.

Takahashi, K., Tanabe, K., Ohnuki, M., Narita, M., Ichisaka, T., To-moda, K., and Yamanaka, S. (2007). Induction of pluripotent stem cells from adult human fibroblasts by defined factors. Cell 131, 861–872.

Teller, S., Granell, C., de Domenico, M., Soriano, J., Gómez, S., and Arenas, A. (2014). Emergence of assortative mixing between clus-ters of cultured neurons. PLoS Comput. Biol. 10, e1003796.

Tibau, E., Ludl, A.-A., Rudiger, S., Orlandi, J.G., and Soriano, J. (2020). Neuronal spatial arrangement shapes effective connectivity traits of *in vitro* cortical networks. IEEE Trans. Netw. Sci. Eng. *7*, 435–448.

Tornero, D., Wattananit, S., Grønning Madsen, M., Koch, P., Wood, J., Tatarishvili, J., Mine, Y., Ge, R., Monni, E., Devaraju, K., et al. (2013). Human induced pluripotent stem cell-derived cortical neurons integrate in stroke-injured cortex and improve functional recovery. Brain *136*, 3561–3577.

Yamamoto, H., Moriya, S., Ide, K., Hayakawa, T., Akima, H., Sato, S., Kubota, S., Tanii, T., Niwano, M., Teller, S., et al. (2018). Impact of modular organization on dynamical richness in cortical networks. Sci. Adv. *4*, eaau4914.